Cleveland State University

EngagedScholarship@CSU

Mechanical Engineering Faculty Publications   Mechanical Engineering Department

2018

Bidirectionally Stretched Flow of Jeffrey Liquid with Nanoparticles, Rosseland Radiation and Variable Thermal Conductivity

M. Archana
Kuvempu University

B. J. Gireesha
Kuvempu University, bjgireesu@gmail.com

M. M. Rashidi
University of Birmingham

B. C. Prasannakumara
Government First Grade College

Rama S.R. Gorla
Cleveland State University, r.gorla@csuohio.edu

Follow this and additional works at: https://engagedscholarship.csuohio.edu/enme_facpub

Part of the Mechanical Engineering Commons

How does access to this work benefit you? Let us know!

Recommended Citation

Bidirectionally stretched flow of Jeffrey liquid with nanoparticles, Rosseland radiation and variable thermal conductivity

M. ARCHANA[a]
B.J. GIREESHA[a*]
M.M. RASHIDI[b]
B.C. PRASANNAKUMARA[c]
R.S.R. GORLA[d]

[a] Department of Studies and Research in Mathematics, Kuvempu University, Shankaraghatta-577451, Shimoga, Karnataka, India

[b] School of Civil Engineering, Birmingham University, Edgbaston Birmingham B15 2TT, United Kingdom

[c] Government First Grade College, Koppa, Chikkamagaluru-577126, Karnataka, India

[d] Department of Mechanical Engineering, Cleveland State University, Cleveland, Ohio-44115, USA

Abstract   Heat and mass transfer stretched flow of an incompressible, electrically conducting Jeffrey fluid has been studied numerically. Nanoparticles are suspended in the base fluid and it has many applications such as cooling of engines, thermal absorption systems, lubricants fuel cell, nanodrug delivery system and so on. Temperature dependent variable thermal conductivity with Rosseland approximation is taken into account and suction effect is employed in the boundary conditions. The governing partial differential equations are first transformed into set of ordinary differential equations using selected similarity transformations, which are then solved numerically using Runge-Kutta-Felhberg fourth-fifth order method along with shooting technique. The flow, heat and mass transfer characteristics with local Nusselt number for various physical parameters are presented graphically and a detailed discussion regarding the effect of flow parame-

*Corresponding Author. Email:bjgireesu@gmail.com

ters on velocity and temperature profiles are provided. It is found that, increase of variable thermal conductivity, radiation, Brownian motion and thermophoresis parameter increases the rate of heat transfer. Local Nusselt number has been computed for various parameters and it is observed that, in the presence of variable thermal conductivity and Rosseland approximation, heat transfer characteristics are higher as compared to the constant thermal conductivity and linear thermal radiation.

Keywords: Heat mass transfer; Jeffrey nanofluid; Variable thermal conductivity; Rosseland approximation; Suction

Nomenclature

a, b	–	constant
B_0	–	uniform magnetic field, $\mathrm{Kg\,S^2 A^1}$
C	–	nanoparticle volume fraction
C_w	–	concentration of nanoparticles at the wall
C_∞	–	ambient nanofluid volume fraction
c	–	stretching rate ratio
$(c_p)_f$	–	specific heat coefficient of fluid, $\mathrm{J/kg\,K}$
$(c_p)_p$	–	specific heat coefficient of nanoparticles, $\mathrm{J/kg\,K}$
D_B	–	Brownian diffusion coefficient, $\mathrm{Kg/m\,s}$
D_T	–	thermophoretic diffusion coefficient, $\mathrm{Kg/m\,sK}$
f, g	–	dimensionless velocity components
k_∞	–	thermal conductivity of the ambient fluid, $\mathrm{W/m\,K}$
k^*	–	mean absorption coefficient, $1/\mathrm{m}$
M	–	magnetic parameter
N_b	–	Brownian motion parameter
Nt	–	thermophoresis parameter
Nu_x	–	local Nusselt number
Pr	–	Prandtl number
Q	–	heat source/sink coefficient
q_r	–	radiative heat flux, $\mathrm{W/m^2}$
Rd	–	thermal radiation parameter
Re_x	–	local Reynolds number
S	–	heat source\sink parameter
Sc	–	Schmidt number
s	–	suction/injection parameter
T	–	fluid temperature, K
T_w	–	fluid temperature at the surface, K
T_∞	–	ambient fluid temperature, K
$k(T)$	–	temperature dependent thermal conductivity, $\mathrm{W/m\,K}$
U_w, V_w	–	velocity of the stretching sheet, m/s
u, v, w	–	velocity components along z, y, and z directions, m/s
W	–	suction/injection velocity, m/s
x, y, z	–	Cartesian coordinates, m

Greek symbols

β –   Deborah number
ε –   variable thermal conductivity
η –   similarity variable
η_∞ –   free stream boundary condition
θ –   dimensionless fluid temperature
θ_w –   temperature ratio parameter
λ_1 –   ratio of relaxation time and retardation time
λ_2 –   retardation time
μ –   dynamic viscosity, Pa s
ν –   kinematic viscosity, m^2/s
ρ_f –   density of the base fluid, kg/m^3
ρ_p –   density of the particles, kg/m^3
ϕ –   dimensionless nanoparticle volume fraction
σ –   electrical conductivity, $1/\Omega m$
σ^* –   Stefan-Boltzmann constant, W/m^2K^4
τ –   ratio of effective heat capacity of the nanoparticle material to heat
                capacity of the fluid

Subscripts and superscripts

w –   conditions at the wall
∞ –   free stream condition
$'$ –   derivative with respect to η

1   Introduction

As an emerging research field, the class of fluids comprised of nanometer-sized additives and base fluids which have been given the name nanofluid have attracted the great attention of researchers for its fascinating thermophysical properties as well as enormous potential applications across the engineering disciplines. The term nanofluid was first introduced by Choi [1]. This type of fluid shows higher thermal performance compared to the base fluids. The model used for the nanofluid incorporates the effects of Brownian motion and thermophoresis. Also, it is interesting to note that, the Brownian motion of nanoparticles at molecular and nanoscale levels is a key nanoscale mechanism governing their thermal behaviour. Keblinski et al. [2] have explored the heat flow mechanisms through the concepts involved in nanofluid such as Brownian motion, heat transfer nature, clustering and liquid layering at the interface of liquid and particle. Control volume based finite element method was been employed by Sheikholeslami et al. [3] to study the nanofluid flow by initiating the magnetic field dependent viscosity. A large number of experimental and theoretical studies have

been carried out by many researchers on thermal conductivity of nanofluid with various effects [4–7] and also many researchers used two phase models [7,8] to present the real phenomenon of heat transfer of nanofluid more precisely. Rashidi *et al.* [9,10] have examined the impact of nanoparticle volume fraction and magnetic field in the nanofluid flow through the vertical channel consisting of sinusoidal walls. Sheikholeslami and Shehzad [11] have considered Kleinstreuer-Li correlation model for nanofluid to study the heat transfer rate of CuO nanoparticle in a porous semi annulus. Kumar *et al.* [12] investigated the impact of cubic autocatalysis chemical reactions in three dimensional flow of nanofluid along a rotating sheet.

During the past few years, research on the boundary layer flow of non-Newtonian fluid becomes a continuous growing part because of its significance in many industrial applications. When fluid stress can have a non-linear or physical dependence on the deformation rate, such materials are referred to as non-Newtonian fluid. These fluids cannot be sufficiently portrayed by the Navier-Stokes theory. Due to the versatility characteristics in the flow behaviour of these fluids in nature, several models have been developed to study their characteristics. Among them Jeffrey model is the simplest non-Newtonian model which possesses the essence of retardation time and the ratio of relaxation to retardation time. Nadeem *et al.* [13] have obtained an analytical solution for the Jeffrey fluid flow and they have studied the configuration of heat transfer in two cases, i.e., prescribed heat transfer (PHT) and prescribed heat flux (PHF) with exponential order in the presence of thermal radiation effect. From the obtained result, it was found that both the cases are qualitatively similar. Hayat *et al.* [14] have investigated the three dimensional Jeffrey fluid flows comprising of temperature dependent variable thermal conductivity by employing homotopy analysis method (HAM). Ashraf *et al.* [15] employed heat and mass convective boundary conditions for the MHD flow of Jeffrey fluid with suspended nanoparticles over a radially stretching surface. An analysis have been carried out by Prasannakumara *et al.* [16] to study the potentialities of enhancing the heat and mass transfer rate in the Jeffrey fluid flow problem with suspended nanoparticles. An analytical description of entropy generation, heat and mass transfer of Casson nanofluid was been explained by Abolbashari *et al.* [17] and they illustrate the increase of entropy generation due to the decrease of Casson parameter through a graph. Ramesh *et al.* [18] discussed the influence of suspended nanoparticles in the boundary layer flow of Maxwell fluid.

Role of radiation heat transfer is superficial in many engineering processes which occur at high temperature. Many authors have studied the effect of Rosseland approximation on heat transfer for both Newtonian and non-Newtonian fluids over stretching surfaces. Mushtaq *et al.* [19] initiated the Rosseland approximation significance in the problem of two-dimensional stagnation-point flow of viscous fluid and analyzed the effect of nonlinear thermal radiation, Joule heating, viscous dissipation in the presence of thermophoresis and Brownian motion which are generated due to nanoparticle suspension. In the presence of nonlinear thermal radiation, characteristics of nanofluid in three dimensional MHD flow problem of Jeffrey fluid was reviewed by Shehzad *et al.* [20]. An emphasis has given on the impact of nonlinear thermal radiation and chemical reaction in two cases, i.e, for constructive and destructive by Prasannakumara *et al.* [21] for the slip flow of non-Newtonian nanofluid and they have determined that, increase of chemical reaction parameter for constructive case decreases the concentration profile whereas opposite behavior exist for the destructive case. Mushtaq *et al.* [22] have constructed a numerical solution for the three dimensional upper convected Maxwell fluid flow and they have obtained S shaped structure in the temperature profile for the larger values of temperature ratio parameter. Besides, applications of suction and injection process can be found in many industrial fields such as thermal oil recovery, wire and fiber coating using polymers, etc. Also the concept of heat source/sink effect has its importance in fluid problems like exothermic/endothermic chemical reactions, geonuclear repositions, etc. Bhattacharya [23] employed finite difference method to analyze the effects of heat source/sink with suction/injection boundary condition for MHD flow of Newtonian fluid over a shrinking sheet. Dinesh and Jat [24] presented their analysis on three dimensional boundary layer flow of viscous fluid over an axisymmetric shrinking sheet and explored the existence conditions for the dual solution in the presence of suction and magnetic parameter. Hayat *et al.* [25] have explained the newly introduced model called Cattaneo-Christov heat flux which assists to overcome the drawbacks of Fourier model in three dimensional Jeffrey fluid flow problem.

In most of the aforesaid literature, thermophysical properties of the fluid such as viscosity, thermal conductivity considered to be are constant. But realistic condition insists these properties to vary significantly with temperature. These changes can be useful and important in improving materials processing systems such as glass fibre production, paper production, wire

drawing and also in lubricating fluids. In order to predict the flow and heat transfer rates relevantly, it becomes crucial to consider the variable fluid properties. An attempt has been made by Megahed [26] to examine the variable properties of the temperature dependent Maxwell fluid flow. Adegbie *et al.* [27] described the dynamics of heat and mass transfer of an upper convected Maxwell fluid by incorporating the variable thermophysical properties and stratification effect. An inspection has been made by Salahuddin *et al.* [28] to scrutinize the consequence of variable thermal conductivity on tangent hyperbolic fluid over a stretching cylinder. Meraj *et al.* [29] discussed the impact of variable thermal conductivity in Jeffrey fluid flow by employing Cattaneo-Christov heat flux model.

The main aim of the present problem is to scrutinize the flow behaviour of Jeffrey nanofluid in the presence of Rosseland approximation and variable thermal conductivity over a permeable stretching surface. Similarity transformations are used to convert the nonlinear partial differential equations to ordinary differential equations. The reduced equations are numerically solved using Runge-Kutta-Fehlberg fourth-fifth order method along with shooting technique. The effect of various parameters have been studied in detail with the help of their graphical representations.

2   Mathematical formulation

Consider a steady, boundary layer flow, heat and mass transfer of an incompressible Jeffrey nanofluid over a permeable stretching surface at $z = 0$. Let $u = U_{\mathrm{w}}(x) = ax$ and $v = V_{\mathrm{w}}(y) = by$ be the velocities of the stretching sheet along the x- and y-directions respectively and the flow occupies the region $z > 0$ as shown in Fig. 1. A constant magnetic field of strength B_0 is applied in the z-direction and induced magnetic field is assumed to be negligible. In the energy equation, Rosseland approximation and heat source/sink effects are considered with variable thermal conductivity which varies linearly in terms of temperature. Under the aforesaid assumptions, the governing basic equations for the present problem are given by [14]

$$\frac{\partial u}{\partial x} + \frac{\partial v}{\partial y} + \frac{\partial w}{\partial z} = 0 \,, \tag{1}$$
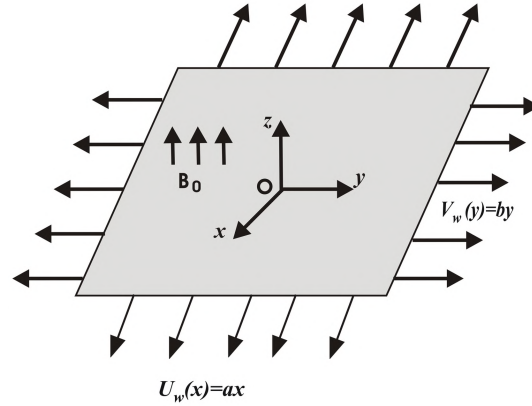
Figure 1: Schematic representation of the flow problem.

$$
u\frac{\partial u}{\partial x} + v\frac{\partial u}{\partial y} + w\frac{\partial u}{\partial z} =
$$

$$
\frac{\nu}{1+\lambda_1}\left[\frac{\partial^2 u}{\partial z^2} + \lambda_2\left(\begin{array}{l}\frac{\partial u}{\partial z}\frac{\partial^2 u}{\partial x\partial z} + \frac{\partial v}{\partial z}\frac{\partial^2 u}{\partial y\partial z} + \frac{\partial w}{\partial z}\frac{\partial^2 u}{\partial z^2} \\ +u\frac{\partial^3 u}{\partial x\partial z^2} + v\frac{\partial^3 u}{\partial y\partial z^2} + w\frac{\partial^3 u}{\partial z^3}\end{array}\right)\right] - \frac{\sigma B_0^2}{\rho}u\ , \quad (2)
$$

$$
u\frac{\partial v}{\partial x} + v\frac{\partial v}{\partial y} + w\frac{\partial v}{\partial z} =
$$

$$
\frac{\nu}{1+\lambda_1}\left[\frac{\partial^2 v}{\partial z^2} + \lambda_2\left(\begin{array}{l}\frac{\partial u}{\partial z}\frac{\partial^2 v}{\partial x\partial z} + \frac{\partial v}{\partial z}\frac{\partial^2 v}{\partial y\partial z} + \frac{\partial w}{\partial z}\frac{\partial^2 v}{\partial z^2} \\ +u\frac{\partial^3 v}{\partial x\partial z^2} + v\frac{\partial^3 v}{\partial y\partial z^2} + w\frac{\partial^3 v}{\partial z^3}\end{array}\right)\right] - \frac{\sigma B_0^2}{\rho}v\ , \quad (3)
$$

$$
u\frac{\partial T}{\partial x} + v\frac{\partial T}{\partial y} + w\frac{\partial T}{\partial z} = \frac{1}{(\rho c)_f}\frac{\partial}{\partial z}\left(k(T)\frac{\partial T}{\partial z}\right) + \tau
$$

$$
\left[D_B\frac{\partial T}{\partial z}\frac{\partial C}{\partial z} + \frac{D_T}{T_\infty}\left(\frac{\partial T}{\partial z}\right)^2\right] - \frac{1}{(\rho c)_f}\frac{\partial q_r}{\partial z} + \frac{Q}{(\rho c)_f}\left(T - T_\infty\right)\ , \quad (4)
$$

$$
u\frac{\partial C}{\partial x} + v\frac{\partial C}{\partial y} + w\frac{\partial C}{\partial z} = D_B\frac{\partial^2 C}{\partial z^2} + \frac{D_T}{T_\infty}\frac{\partial^2 T}{\partial z^2}, \quad (5)
$$

where u, v, and w are the velocity components along the x, y, and z-direction, respectively, $\nu = \frac{\mu}{\rho}$ is the kinematic viscosity of the fluid, μ is the coefficient of fluid viscosity ρ is the fluid density, σ is the electrical conductivity of the fluid, $k(T)$ is the temperature dependent variable thermal conductivity, c_f and c_p are the specific heat coefficient of fluid and

nanoparticles, respectively, ρ_f and ρ_p are the densities of the base fluid and nanoparticles respectively, $\tau = \frac{(\rho c)_p}{(\rho c)_f}$ is the ratio of effective heat capacity of the nanoparticle material to heat capacity of the fluid, D_B is the Brownian diffusion coefficient, D_T is the thermophoretic diffusion coefficient, q_r is the radiative heat flux, Q is the heat source/sink coefficient, T is the fluid temperature and C is the concentration of the fluid.

The associated boundary conditions for the current problem are given by

$$\left. \begin{array}{l} u = ax, \quad v = by, \quad w = W, \quad T = T_w, \quad C = C_w \quad \text{at} \quad z = 0 \\ u \to 0, \quad v \to 0, \quad T \to T_\infty, \quad C \to C_\infty \qquad \text{as} \quad z \to \infty, \end{array} \right\} , \quad (6)$$

where $W > 0$ is the suction velocity, T_w and T_∞ are the temperature at the wall and ambient fluid temperature respectively, C_w and C_∞ are the concentration of the nanoparticles at the wall and far away from the surface respectively, a and b are constant rate having the dimension inverse of time.

Rosseland approximation is applicable only inside optically dense media at large optical distances from the boundaries and from regions with strong variation of temperature and medium properties. Using the Rosseland approximation for radiation, radiation heat flux is simplified as

$$q_r = -\frac{4\sigma^*}{3k^*}\frac{\partial T^4}{\partial z} = -\frac{16\sigma^*}{3k^*}T^3\frac{\partial T}{\partial z} , \quad (7)$$

where σ^* and k^* are the Stefan-Boltzmann constant and the mean absorption coefficient respectively.

Variation of thermal conductivity with respect to temperature can be written as

$$k(T) = k_\infty \left(1 + \varepsilon \frac{T - T_\infty}{T_w - T_\infty} \right) , \quad (8)$$

where k_∞ is the thermal conductivity of the ambient fluid and ε is the variable thermal conductivity parameter.

The momentum, energy and concentration equations can be transformed into the corresponding ordinary differential equations using the following similarity variables

$$u = axf'(\eta) , \quad v = ayg'(\eta) , \quad w = -\sqrt{a\nu}[f(\eta) + g(\eta)] , \quad (9)$$

$$T = T_\infty [1 + (\theta_w - 1)\theta(\eta)] , \quad \phi(\eta) = \frac{C - C_\infty}{C_W - C_\infty}, \quad \eta = \sqrt{\frac{a}{\nu}}z , \quad (10)$$

where $\theta_w = \frac{T_w}{T_\infty}$, $\theta_w > 1$ being the temperature ratio parameter.

Now, we can see that the Eq. (2) is automatically satisfied, and Eqs. (3)–(6) are reduced as follows:

$$f''' + (1 + \lambda_1)\left[(f + g) f'' - f'^2\right]$$
$$+ \beta\left[f''^2 - (f + g) f'''' - g'f'''\right] - (1 + \lambda_1) Mf' = 0, \qquad (11)$$

$$g''' + (1 + \lambda_1)\left((f + g) g'' - g'^2\right)$$
$$+ \beta\left[g''^2 - (f + g) g'''' - f'g'''\right] - (1 + \lambda_1) Mg' = 0, \qquad (12)$$

$$\left[1 + \varepsilon\theta + Rd(1 + (\theta_w - 1)\theta)^3\right]\theta'' + \varepsilon\theta'^2 + 3Rd\left[1 + (\theta_w - 1)\theta\right]^2 (\theta_w - 1)\theta'^2$$
$$+ \Pr\left[(f + g)\theta' + N_b\theta'\phi' + N_t\theta'^2 + S\theta\right] = 0, \qquad (13)$$

$$\phi'' + Sc(f + g)\phi' + \frac{N_t}{N_b}\theta'' = 0, \qquad (14)$$

and corresponding boundary conditions becomes

$$f = s, \ g = 0, \ f' = 1, \ g' = c, \ \theta(0) = 1, \ \phi(0) = 1 \ \text{at} \ \eta = 0,$$
$$f' \to 0, \ g' \to 0, \ \theta \to 0, \ \phi \to 0 \ \text{as} \ \eta \to \infty, \qquad (15)$$

where $\beta = \lambda_2 a$ is the Deborah number, $M = \frac{\sigma B_0^2}{\rho a}$ is the magnetic parameter, $\Pr = \frac{\nu(\rho c)_f}{k_\infty}$ is the Prandtl number, $Rd = \frac{16\sigma^* T_\infty^3}{3k_\infty k^*}$ is the radiation parameter, $N_b = \frac{\tau D_B(C_w - C_\infty)}{\nu}$ is the Brownian motion parameter, $N_t = \frac{\tau D_T(T_w - T_\infty)}{\nu T_\infty}$ is the thermophoresis parameter, $S = \frac{Q}{a(\rho c)_f}$ is the heat source/sink parameter, $Sc = \frac{\nu}{D_B}$ is the Schmidt number, $s = -\frac{W}{\sqrt{a\nu}}$ is the suction/injection parameter, $c = \frac{b}{a}$ is the ratio of stretching rates and a prime stands for differentiation with respect to η.

The quantities of practical interest is the local Nusselt number which is described as follows:

$$\mathrm{Nu}_x = \frac{x}{k_\infty(T_w - T_\infty)}\left[-k(T)\frac{\partial T}{\partial z} + (q_r)_w\right],$$

$$(\mathrm{Re}_x)^{-\frac{1}{2}}\mathrm{Nu}_x = -\left[1 + \varepsilon\theta(0) + Rd\theta_w^3\right]\theta'(0),$$

where $\mathrm{Re}_x = \frac{U_w^2}{a\nu}$ is the local Reynolds number.

3   Numerical method

The system of coupled nonlinear ordinary differential equations (12)–(15) along with the boundary conditions (16) is solved numerically using Runge--Kutta–Fehlberg fourth-fifth order method (RKF-45 method) along with shooting technique. The efficiency of this method is enhanced due to the reduction of computational time. With the help of shooting technique, missed initial conditions are inferred. Shooting technique is an iterative algorithm which attempts to identify appropriate initial conditions for a relevant initial value problem that provides the solution to the original boundary value problem. We have considered infinity condition at a large but finite value of η, where negligible variation in velocity, temperature and so on occurs.

After fixing finite value for η_∞, integration is carried out with the help of Runge-Kutta-Fehlberg-45 method. This method has a procedure to determine an accurate solution if the proper step size is being used. At each step, two different approximations for the solution are made and compared. If the two answers are in close agreement, the approximation is accepted otherwise the step size is reduced until to get the required accuracy. For the present problem, we took step size $\Delta\eta = 0.001$, $\eta_\infty = 5$ and accuracy to the fifth decimal place.

To have a check on the accuracy of the numerical approach used, we have computed $f''(0)$ and $g''(0)$ that are carried out for viscous fluid for various values of stretching rate parameter and compared with the available published results of Liu and Anderson [30] and Mushtaq et $al.$ [31] in Tab. 1 and they are found to be in excellent agreement.

Table 1: Comparison table for $-f''(0)$ and $-g''(0)$ with $\lambda_1 = 0$, $\beta = 0$, $M = 0$.

c	Liu and Anderson [30]		Mushtaq et $al.$ [31]		Present (RKF45 Method)	
	$-f''(0)$	$-g''(0)$	$-f''(0)$	$-g''(0)$	$-f''(0)$	$-g''(0)$
0.00	1	0	1	0	1	0
0.25	1.048813	0.194565	1.048811	0.194564	1.048834	0.194565
0.50	1.093096	0.465206	1.093095	0.465205	1.093105	0.465206
0.75	1.134486	0.794619	1.134486	0.794618	1.134491	0.794615
1.00	1.173721	1.173721	1.173721	1.173721	1.173723	1.173721

4 Result and discussions

In this section clear insight of velocity, temperature and concentration profiles are analyzed for various physical parameters through graphs 2–15 in detail.

Figures 2–4 illustrates the role of the Deborah number (β), ratio of relaxation and retardation times (λ_1), magnetic parameter (M), stretching rate parameter (c), suction/injection parameter (s) on velocity profiles. The variation of velocity profiles for β and λ_1 can be visually represented in Fig. 2. As Deborah number depends on retardation time, which makes the velocity to increase, fluid velocity profile and corresponding boundary layer thickness must increase. Also ratio of relaxation and retardation times exhibits the characteristics of viscous as well as elastic in aspect. Hence, whenever viscosity or elasticity increases, flow of the fluid velocity decreases.
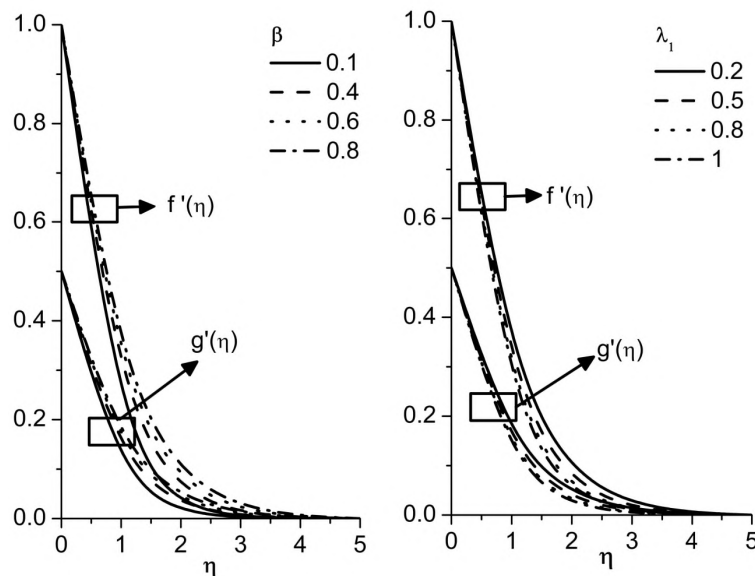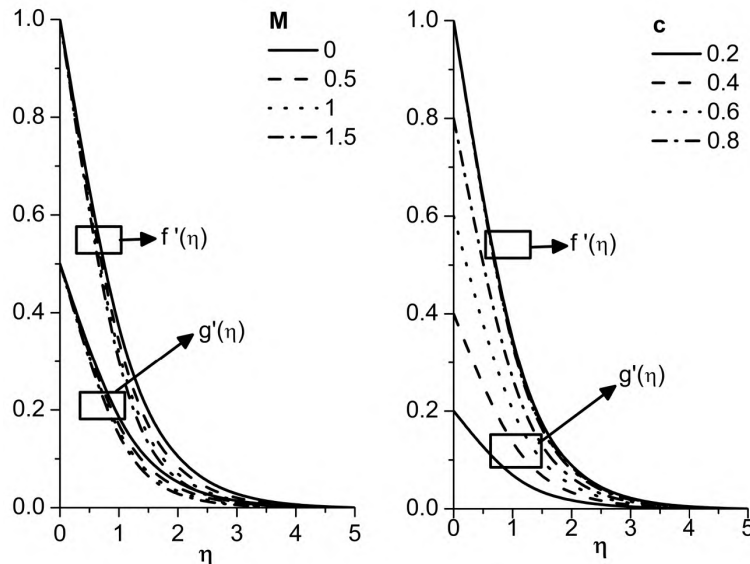

Figure 2: Influence of β and λ_1 on $f'(\eta)$ and $g'(\eta)$.

Figure 3 preserves the effect of M and c on velocity profile. We can notice from the Fig. 3 that, velocity profile and corresponding momentum boundary layer is a decreasing function of magnetic parameter. It is because of the fact of Lorentz force generated by magnetic field, which retards the

Figure 3: Influence of M and c on $f'(\eta)$ and $g'(\eta)$.

fluid flow. Also it is found that, the velocity profile $f'(\eta)$ and the thickness of associated boundary layer thickness decreases, when the stretching rate parameter increases. Consequently, $g'(\eta)$ exhibits the opposite behavior for the same parameter. This is because, as the stretching rate parameter describes the ratio of axial and transverse stretching, with the increase of c, velocity coefficient of x component decreases where as the lateral surface is moving along y-direction. Hence the velocity profile $f'(\eta)$ decreases while $g'(\eta)$ increases. It is found from Fig. 4 that, the velocity profile and the thickness of associated boundary layer decreases for $s > 0$ and increases for $s < 0$. Increasing of this parameter drags the fluid particles close to the wall which causes the velocity profile to decrease.

Figures 5–11 display several temperature and concentration profiles for variable thermal conductivity (ε), Brownian motion parameter (Nb), thermophoresis parameter (Nt), radiation parameter (Rd), Prandtl number (Pr), temperature ratio parameter (θ_w), uniform heat source/sink parameter (S) in the presence of constant and temperature dependent variable thermal conductivity as well as in the presence of linear and nonlinear thermal radiation.

The influence of Brownian motion and thermophoresis parameter on temperature profile can be visualized through Figs. 5 and 6. These param-
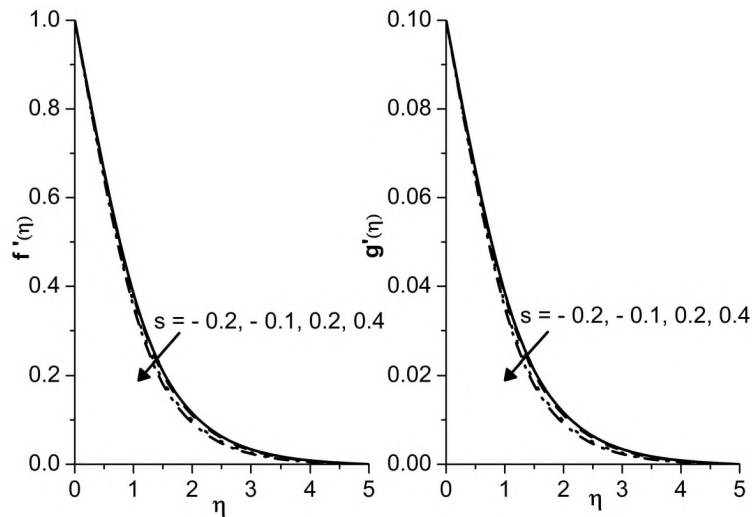
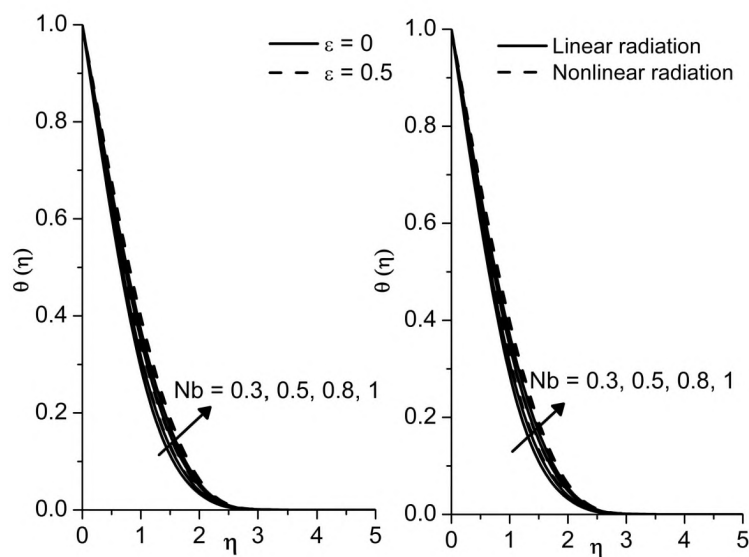Figure 4: Influence of s on $f'(\eta)$ and $g'(\eta)$.

Figure 5: Comparative result of influence of Nb on $\theta(\varepsilon)$ when $\varepsilon = 0.0.5$ and $\theta_w = 1, > 1$.

eters represent the presence of nanoparticles in the fluid. As the nanoparticles enhance the thermal conductivity of the fluid, it leads to higher temperature and thicker thermal boundary layer. It is clear from the Fig. 7 that,
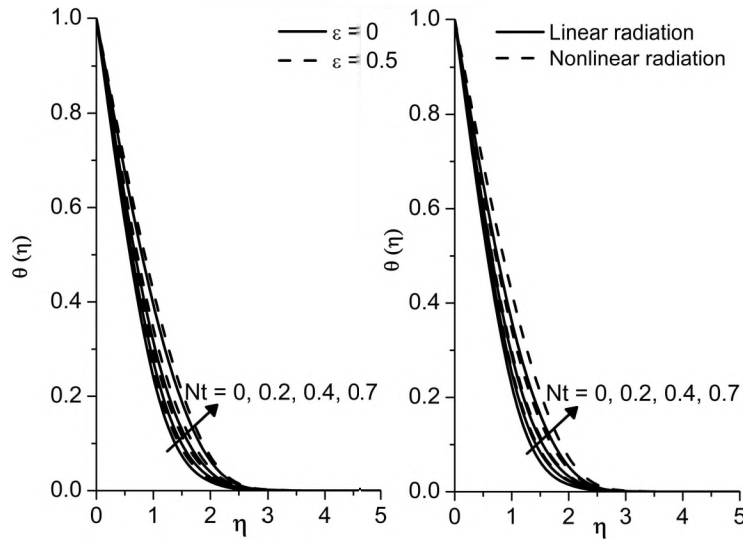
Figure 6: Comparative result of influence of Nt on $\theta(\eta)$ when $\varepsilon = 0.0.5$ and $\theta_w = 1, > 1$.
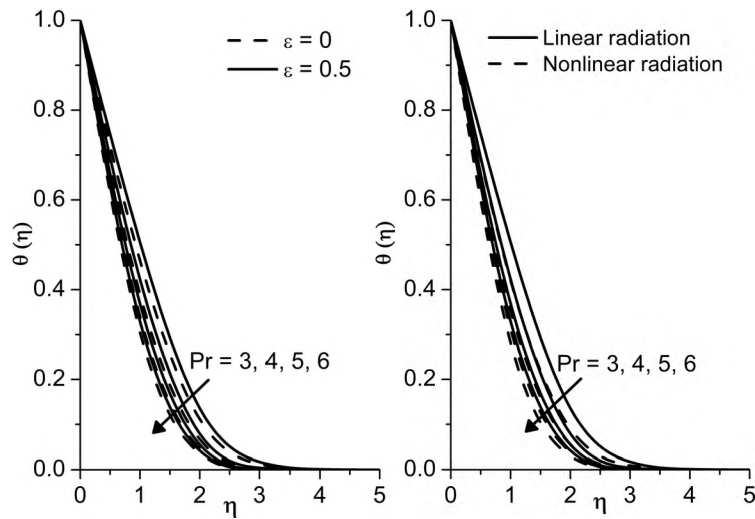

Figure 7: Comparative result of influence of Pr on $\theta(\eta)$ when $\varepsilon = 0.0.5$ and $\theta_w = 1, > 1$.

thickness of the thermal boundary layer and temperature are decreasing functions of Pr. This is because as the Prandtl number increases, thermal diffusivity decreases there by decreases the temperature.

The description of heat source/sink parameter for the temperature pro-

file can be viewed through the Fig. 8. It is evident from these figures that the temperature profile increases for $S > 0$ and decreases for $S < 0$ due to the fact that increase of this parameter generates more heat within the boundary layer. Figure 9 exhibits the variation of temperature profile for the radiation parameter. As the radiation parameter releases the heat energy into the flow, with an increase of radiation parameter, temperature profile increases.
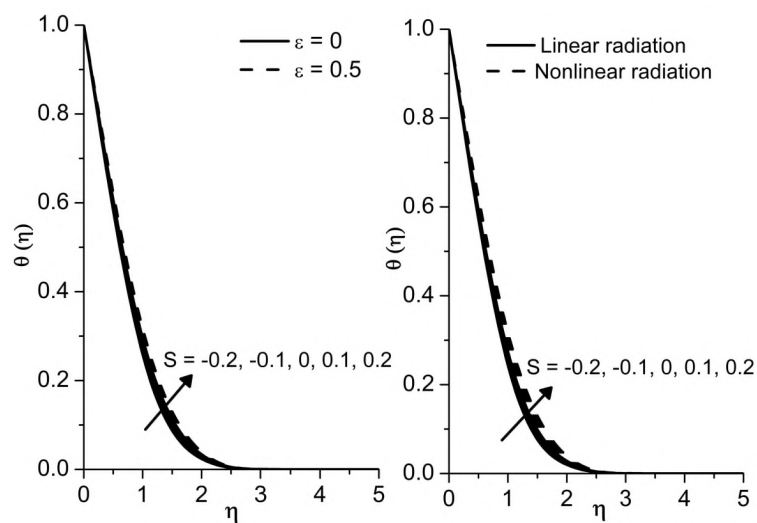

Figure 8: Comparative result of influence of S on $\theta(\eta)$ when $\varepsilon = 0.0.5$ and $\theta_w = 1, > 1$.

Figure 10 portraits that, temperature profile is an increasing function of temperature ratio parameter and variable thermal conductivity parameter. This phenomenon occurs because temperature ratio parameter describes the thermal state of the fluid and with the increase of this parameter temperature also increases. Further, increase of ε leads to increase in the wall temperature which makes the temperature profile to increase.

Figure 11 elucidates the effect of Brownian motion and thermophoresis parameter on concentration profile. It reveals that, as N_b and N_t increases, concentration and the associated boundary layer thickness decreases for the parameter N_b while it increases for N_t. Impact of Schmidt number on concentration profile can be viewed through Fig. 12. Since Schmidt number depends on the Brownian diffusion coefficient, larger values of Schmidt number makes the Brownian diffusion coefficient as lower, which shows
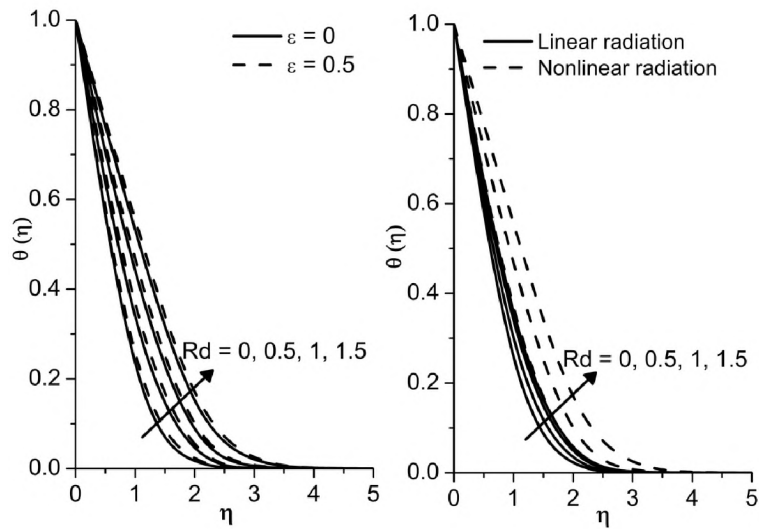
Figure 9: Comparative result of influence of Rd on $\theta\left(\eta\right)$ when $\varepsilon = 0.0.5$ and $\theta_w = 1, > 1$.
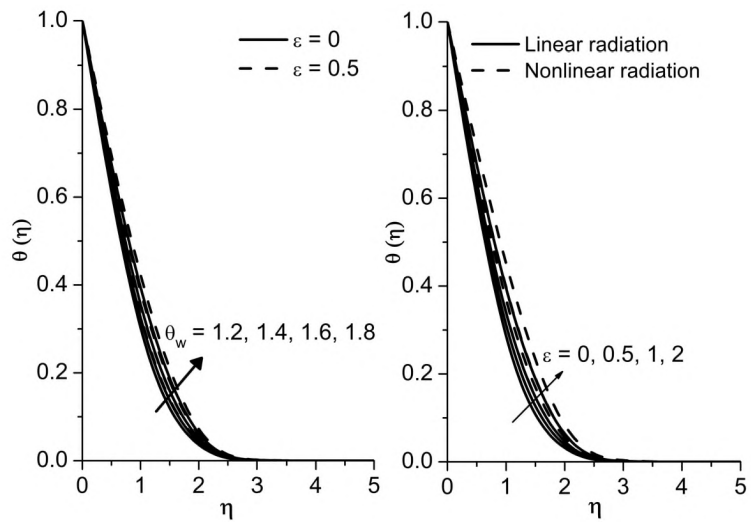
Figure 10: Comparative result of influence θ_w and ε parameter on $\theta\left(\eta\right)$ when $\varepsilon = 0.0.5$ and $\theta_w = 1, > 1$.

a weaker nanoparticle concentration.

Figure 13 elucidate the effect of ε with θ_w on local Nusselt number. It is observed that, local Nusselt number increases for increasing values

Figure 11: Influence of Nb and Nt parameter on $\phi\left(\eta\right)$.

Figure 12: Influence of Sc on $\phi(\eta)$.

of variable thermal conductivity with temperature ratio parameter. The influence of Brownian motion with thermophoresis parameter on Nusselt

and Sherwood number are depicted in Figs. 14 and 15, respectively. From these figures, it is observed that, Nusselt and Sherwood number decreases for increasing values of N_b with N_t.
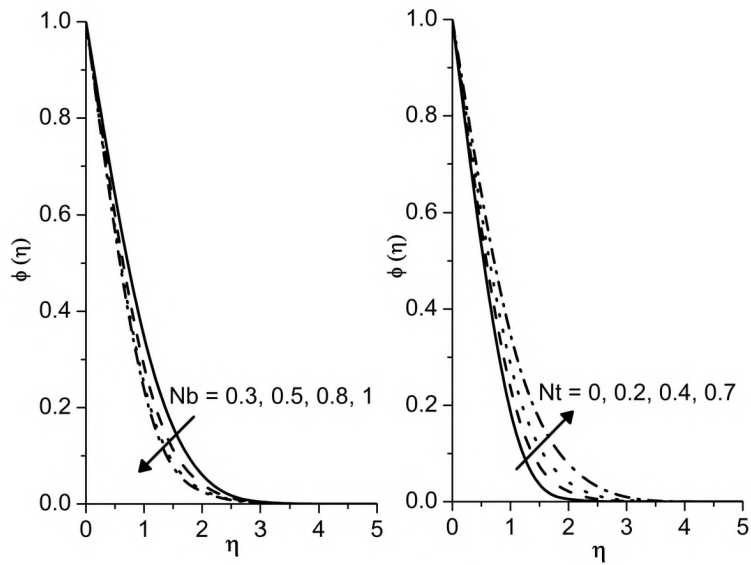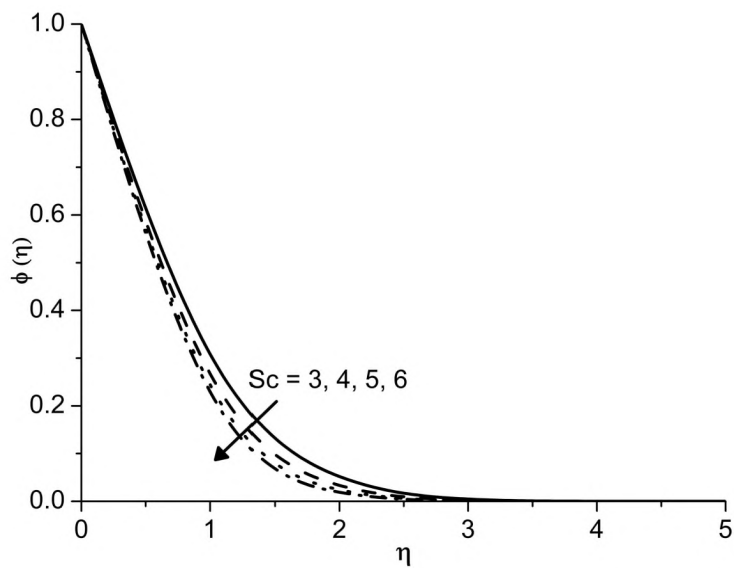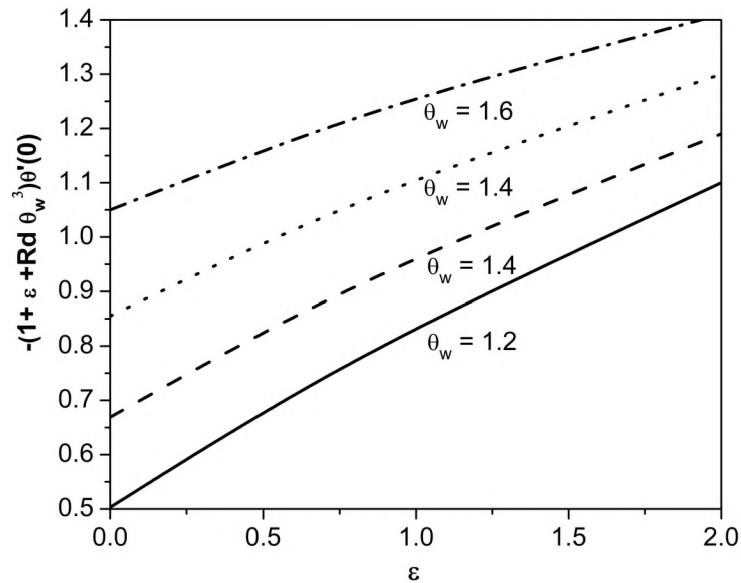

Figure 13: Influence of ε with θ_w for Nusselt number.

The numerical values of local Nusselt number for various values of the parameters M, β, λ_1, c, N_b, N_t, Pr, Rd, θ_w, s, S, ε, and Sc are manifested in Tabs. 2, 3 and 4. For the varying values of M, λ, N_b N_t S, Sc, the rate of heat transfer at the surface decreases whereas it increases for the increasing parameters of β, c, Pr, Rd, θ_w and s. It is evident from the Tabs. 2 and 3 that, in the presence of variable thermal conductivity and nonlinear thermal radiation, local Nusselt number are higher compared to the constant thermal conductivity and linear thermal radiation. Also from Tab. 4, we can observe that the influence of variable thermal conductivity parameter increases the Nusselt number values in the presence of linear thermal radiation and decreases for the non-linear thermal radiation effect.

Table 2: Comparative numerical values of local Nusselt number for various physical parameters for constant and variable thermal conductivity.

M	β	λ_1	c	N_b	N_t	Pr	Rd	θ_w	s	S	Sc	$(\mathrm{Re}_x)^{-\frac{1}{2}}\mathrm{Nu}_x$ when $\varepsilon = 0.5$	$(\mathrm{Re}_x)^{-\frac{1}{2}}\mathrm{Nu}_x$ when $\varepsilon = 0$
0	0.5	0.5	0.5	0.5	0.5	5	0.5	1.5	0.5	0.5	3	0.971577	0.811147
0.5												0.907371	0.760033
1												0.849021	0.713643
0.5	0.1											0.715370	0.608763
	0.2											0.786048	0.664247
	0.4											0.876136	0.735326
	0.5	0.3										0.948096	0.792362
		0.6										0.887415	0.744195
		0.9										0.828733	0.697653
		0.5	0.2									0.619091	0.514846
			0.4									0.820754	0.686205
			0.8									1.130819	0.950682
			0.5	0.3								1.333006	1.193023
				0.6								0.733670	0.587773
				0.8								0.45126	0.315645
				0.5	0							1.697291	1.526537
					0.3							1.188903	1.029201
					0.6							0.779759	0.639626
					0.5	3						0.820752	0.747077
						4						0.902694	0.785106
						5						0.907371	0.760033
						5	0					0.294932	0.084841
							0.4					0.804288	0.643528
							0.8	1.5				1.162747	1.051992
							0.5	1.3				0.750980	0.582742
							0.5	1.6				0.990934	0.854943
								1.8				1.162358	1.050206
								1.5	0.3			0.153459	0.084835
									0.4			0.672218	0.547971
									0.6			1.133919	0.965067
									0.5	-0.2		2.179125	1.910334
										0		1.868401	1.62748
										0.2		1.523706	1.314795
										0.5	2	0.996502	0.864960
											4	0.873187	0.717457
											5	0.858025	0.697214

Table 3: Comparative numerical values of local Nusselt number for various physical parameters for Linear and Nonlinear thermal radiation.

| M	β	λ_1	c	N_b	N_t	Pr	Rd	θ_w	s	S	Sc	$(\mathrm{Re}_x)^{-\frac{1}{2}}\mathrm{Nu}_x$	$(\mathrm{Re}_x)^{-\frac{1}{2}}\mathrm{Nu}_x$
0	0.5	0.5	0.5	0.5	0.5	5	0.5	1.5	0.5	0.5	3	0.971577	0.594313
0.5												0.907371	0.557577
1												0.849021	0.524180
0.5	0.1											0.715370	0.449471
	0.2											0.786048	0.489096
	0.4											0.876136	0.539919
	0.5	0.3										0.948096	0.580741
		0.6										0.887415	0.546213
		0.9										0.828733	0.512770
		0.5	0.2									0.619091	0.363774
			0.4									0.820754	0.499222
			0.8									1.130819	0.707952
			0.5	0.3								1.333006	0.998068
				0.6								0.733670	0.390033
				0.8								0.451260	0.139579
				0.5	0							1.697291	1.283361
					0.3							0.61.188903	0.806279
												0.779759	0.448774
					0.5	3						0.820752	0.623965
						4						0.902694	0.614403
						5						0.907371	0.557577
						5	0					0.294932	0.294932
							0.4					0.804288	0.508054
							0.8	1.5				1.162747	0.696056
							0.5	1.3				0.750980	–
								1.6				0.990934	–
								1.8				1.162358	–
								1.5	0.3			0.153459	0.186159
									0.4			0.672218	0.375828
									0.6			1.133919	0.734108
									0.5	-0.2		2.179125	1.555428
										0		1.868401	1.308182
										0.2		1.523706	1.036070
										0.5	2	0.996502	0.683698
											4	0.873187	0.503263
											5	0.858025	0.475618
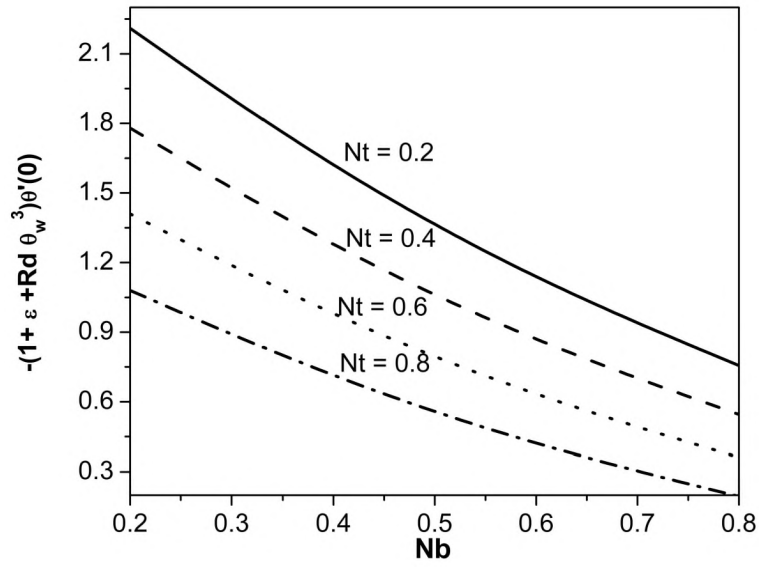
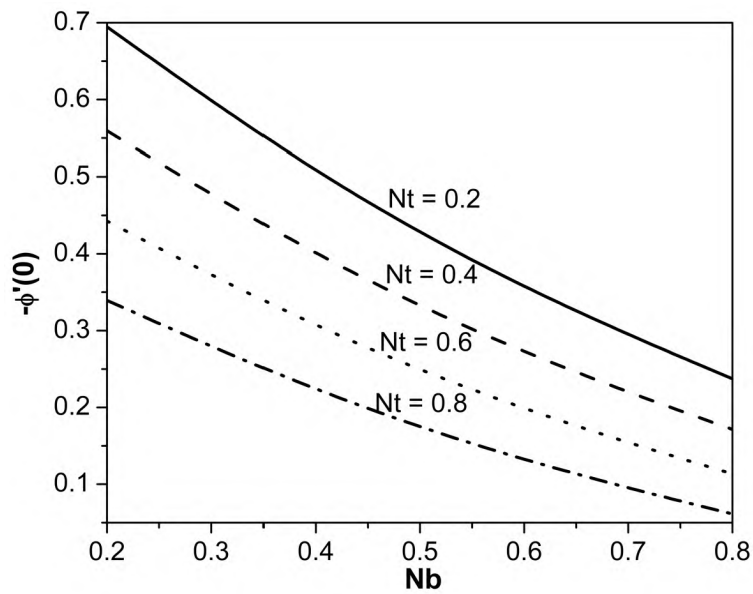Figure 14: Influence of N_b with N_t for Nusselt number.

Figure 15: Influence of N_b with N_t for Sherwood number.

Table 4: Numerical values of local Nusselt number for variable thermal conductivity parameter

ε	$(\mathrm{Re}_x)^{-\frac{1}{2}}\,\mathrm{Nu}_x$	$(\mathrm{Re}_x)^{-\frac{1}{2}}\,\mathrm{Nu}_x$
0.3	0.907606	0.48306
0.5	0.907371	0.557577
1.0	0.896329	0.728886

5   Conclusion

The effect of variable thermal conductivity on Jeffrey nanofluid flow under the influence of magnetohydrodynamic and nonlinear thermal radiation effect is studied over a porous stretching sheet. The impact of various non dimensionless parameters are investigated through graphs and table and corresponding results are summarized as follows:

1. Velocity profiles increases with increase in Deborah number while it decreases for increasing value of magnetic, ratio of relaxation time to retardation time and suction/injection parameter.

2. Velocity profile $g'(\eta)$ and corresponding momentum boundary layer thickness increases with increase in stretching rate parameter, whereas velocity profile $f'(\eta)$ exhibits opposite behaviour for the same parameter.

3. Thermal boundary layer is thicker for the effect of variable thermal conductivity parameter, Brownian motion parameter, thermophoresis parameter, radiation parameter, temperature ratio parameter, heat source/sink parameter.

4. Temperature profile decreases with increasing values of Prandtl number.

5. Concentration boundary layer thickness is a decreasing function of Brownian motion parameter, Schmidt number whereas increasing function for thermophoresis parameter.

6. Variable thermal conductivity and nonlinear thermal radiation effect have strong influence on heat transfer characteristics.

7. Local Nusselt number increases for increasing values of variable thermal conductivity with temperature ratio parameter whereas for Brownian motion with thermophoresis parameter both Nusselt number and Sherwood number decreases.

8. Due to increasing global competitiveness, a number of industries have a strong need to supplement advanced heat transfer fluids with significantly higher thermal conductivities than are presently accessible. As an example we can consider the radiators in vehicles which are designed to cool the engine with continuous heat transfer. A significant energy savings can be made by incorporating the model of the nanofluid in such heat exchangers. Further, the behavior of non-Newtonian fluids is encountered in almost all the chemical and allied processing industries. Among them, Jeffrey fluid shows the linear viscoelastic effect of fluid which has many applications in polymer industries. One of the examples of Jeffrey fluid includes dilute polymer solution.

References

[1] CHOI S.U.S., EASTMAN J.A.: *Enhancing thermal conductivity of fluids with nanoparticles.* ASME FED. 231/MD **66**(1995), 99–105.

[2] KEBLINSKI P., PHILLPOT S.R., CHOI S.U.S., EASTMAN J.A.: *Mechanisms of heat flow in suspensions of nano-sized particles (nanofluids).* Int. J. Heat Mass Tran. **45**(2002), 4, 855–863.

[3] SHEIKHOLESLAMI M., RASHIDI M.M., HAYAT T., GANJI D.D.: *Free convection of magnetic nanofluid considering MFD viscosity effect.* J. Mol. Liq. **218**(2016), 393–399.

[4] REDDY M.G.: *Influence of magnetohydrodynamic and thermal radiation boundary layer flow of a nanofluid past a stretching sheet.* J. Sci. Res. **6**(2014), 2, 257–272.

[5] RUP K., NERING K: *Unsteady natural convection in micropolar nanofluids.* Arch. Thermodyn. **35**(2014), 3, 155–170.

[6] ABBAS Z., NAVEEDA M., SAJID M.: *Hydromagnetic slip flow of nanofluid over a curved stretching surface with heat generation and thermal radiation.* J. Mol. Liq. **215**(2016), 756–762.

[7] VEENA P.H., BIRADAR S.M., NANDEPPANAVAR M.M.: *Free convection boundary layer flow and heat transfer of a nano fluid over a moving plate with internal heat generation.* Ind. Eng. Lett. **6** (2016), 2, 39–49.

[8] BEG O.A., RASHIDI M.M., AKBARI M., HOSSEINI A.: *Comparative numerical study of single-phase and two-phase models for bio-nanofluid transport phenomena.* J. Mech. Med. Biol. **14**(2014), 1, 1450011.

[9] GAROOSI F., BAGHERI G., RASHIDI M.M.: *Two phase simulation of natural convection and mixed convection of the nanofluid in a square cavity.* Powder Technol. **275**(2015), 239–256.

[10] RASHIDI M.M., NASIRI M., KHEZERLOO M., LARAQI N.:*Numerical investigation of magnetic field effect on mixed convection heat transfer of nanofluid in a channel with sinusoidal walls.* J. Magn. Magn. Mater. **93**(2016), 674–682.

[11] SHEIKHOLESLAMI M., SHEHZAD S.A.: *Magnetohydrodynamic nanofluid convection in a porous enclosure considering heat flux boundary condition.* Int. J. Heat Mass Tran. **106**(2017), 1261–1269.

[12] KUMAR R., SOOD S., SHEIKHOLESLAMI M., SHEHZAD S.A.: *Nonlinear thermal radiation and cubic autocatalysis chemical reaction effects on the flow of stretched nanofluid under rotational oscillations.* J. Colloid Interf. Sci. **505**(2017) 253–265.

[13] NADEEM S., ZAHEER S., FANG T.: *Effects of thermal radiation on the boundary layer flow of a Jeffrey fluid over an exponentially stretching surface.* Numer. Algor. **57**(2011), 187–205.

[14] HAYAT T., SHEHZAD S.A., ALSAEDI A.: *Three-dimensional stretched flow of Jeffrey fluid with variable thermal conductivity and thermal radiation,* Appl. Math. Mech.-Engl. **34** (2013), 7, 823–832.

[15] ASHRAF M.B., HAYAT T., ALSAEDI A., SHEHZAD S.A.: *Convective heat and mass transfer in MHD mixed convection flow of Jeffrey nanofluid over a radially stretching surface with thermal radiation.* J. Cent. South Univ. **22**(2015), 1114–1123.

[16] PRASANNAKUMARA B.C., KRISHNAMURTHY M.R., GIREESHA B.J., GORLA R.S.R.: *Effect of multiple slips and thermal radiation on MHD flow of Jeffery nanofluid with heat transfer.* J. Nanofluids. **5**(2016), 82–93.

[17] ABOLBASHARI M.H., FREIDOONIMEHR N., NAZARI F., RASHIDI M.M.: *Analytical modeling of entropy generation for Casson nano-fluid flow induced by a stretching surface.* Adv. Powder Technol. **26**(2015), 2, 542–552.

[18] RAMESH G.K., PRASANNAKUMARA B.C., GIREESHA B.J., SHEHZAD S.A., ABBASI F.M.: *Three dimensional flow of Maxwell fluid with suspended nanoparticles past a bidirectional porous stretching surface with thermal radiation.* Therm. Sci. Eng. Prog. **1**(2017), 6–14.

[19] MUSHTAQ A., MUSTAFA M., HAYAT T., ALSAEDI A.: *Nonlinear radiative heat transfer in the flow of nanofluid due to solar energy: A numerical study.* J. Taiwan Inst. Chem. Eng. **45**(2014), 4, 1176–1183.

[20] SHEHZAD S.A., HAYAT T., ALSAEDI A., OBID M.A.: *Nonlinear thermal radiation in three-dimensional flow of Jeffrey nanofluid: A model for solar energy.* Appl. Math. Comp. **248**(2014), 273–286.

[21] PRASANNAKUMARA B.C., GIREESHA B.J., GORLA R.S.R., KRISHNAMURTHY M.R.: *Effects of chemical reaction and nonlinear thermal radiation on Williamson nanofluid slip flow over a stretching sheet embedded in a porous medium.* J. Aerospace Eng. **29**(2016), 5, 04016019.

[22] MUSHTAQ A., MUSTAFA M., HAYAT T., ALSAEDI A.: *A numerical study for three-dimensional viscoelastic flow inspired by non-linear radiative heat flux.* Int. J. Non-linear Mech. **79**(2016), 83–87.

[23] BHATTACHARYYA K.: *Effects of radiation and heat source/sink on unsteady MHD boundary layer flow and heat transfer over a shrinking sheet with suction/injection.* Front. Chem. Sci. Eng. **5** (2011), 3, 376–384.

[24] RAJOTIA D., JAT R.N.: *Dual solutions of three dimensional MHD boundary layer flow and heat transfer due to an axisymmetric shrinking sheet with viscous dissipation and heat generation/absorption.* Indian J. Pure Appl. Phys. **52**(2014), 812–820.

[25] HAYAT T., QAYYUM S., IMTIAZ M., ALSAEDI A.: *Three-dimensional rotating flow of Jeffrey fluid for Cattaneo-Christov heat flux model.* AIP Adv. **6**(2016), 025012:1-12.

[26] MEGAHED A.M.: *Variable fluid properties and variable heat flux effects on the flow and heat transfer in a non-Newtonian Maxwell fluid over an unsteady stretching sheet with slip velocity.* Chin. Phys. B. **22**(2013), 9, 094701:1–6.

[27] ADEGBIE K.S., OMOWAYE A.J., DISU A.B., ANIMASAUN I.L.: *Heat and mass transfer of upper convected Maxwell fluid flow with variable thermo-physical properties over a horizontal melting surface.* Appl. Math. **6**(2015), 1362–1379.

[28] SALAHUDDIN T., MALIK M.Y., HUSSAIN A., BILAL S., AWAIS M.: *Effects of transverse magnetic field with variable thermal conductivity on tangent hyperbolic fluid with exponentially varying viscosity.* AIP Adv. **5**(2015), 127103:1–14.

[29] MERAJ M.A., SHEHZAD S.A., HAYAT T., ABBASI F.M., ALSAEDI A.: *Darcy-Forchheimer flow of variable conductivity Jeffrey liquid with Cattaneo-Christov heat flux theory.* Appl. Math. Mech.-Engl. **38**(2017), 4, 557–566.

[30] LIU I.C., ANDERSSON H.I.: *Heat transfer over a bidirectional stretching sheet with variable thermal conditions.* Int. J. Heat Mass Tran. **51**(2008), 4018–4024.

[31] MUSHTAQ A., MUSTAFA M., HAYAT T., ALSAEDI A.: *A numerical study for three-dimensional viscoelastic flow inspired by non-linear radiative heat flux.* Int. J. Non-linear Mech. **79** (2016), 83–87.